

Effect of Structural Heterogeneity on *In Situ* Deformation of Dissimilar Weld Between Ferritic and Austenitic Steel



M. GHOSH, R. SANTOSH, S.K. DAS, G. DAS, B. MAHATO, J. KORODY, S. KUMAR, and P.K. SINGH

Low-alloy steel and 304LN austenitic stainless steel were welded using two types of buttering material, namely 309L stainless steel and IN 182. Weld metals were 308L stainless steel and IN 182, respectively, for two different joints. Cross-sectional microstructure of welded assemblies was investigated. Microhardness profile was determined perpendicular to fusion boundary. *In situ* tensile test was performed in scanning electron microscope keeping low-alloy steel-buttering material interface at the center of gage length. Adjacent to fusion boundary, low-alloy steel exhibited carbon-depleted region and coarsening of matrix grains. Between coarse grain and base material structure, low-alloy steel contained fine grain ferrite-pearlite aggregate. Adjacent to fusion boundary, buttering material consisted of Type-I and Type-II boundaries. Within buttering material close to fusion boundary, thin cluster of martensite was formed. Fusion boundary between buttering material-weld metal and weld metal-304LN stainless steel revealed unmixed zone. All joints failed within buttering material during *in situ* tensile testing. The fracture location was different for various joints with respect to fusion boundary, depending on variation in local microstructure. Highest bond strength with adequate ductility was obtained for the joint produced with 309L stainless steel-buttering material. High strength of this weld might be attributed to better extent of solid solution strengthening by alloying elements, diffused from low-alloy steel to buttering material.

DOI: 10.1007/s11661-015-2930-4

© The Minerals, Metals & Materials Society and ASM International 2015

I. INTRODUCTION

DISSIMILAR metals welded joint (DMW) between low-alloy steel and austenitic stainless steel is widely used as primary piping of heat transport system in pressurized water reactors (PWR) of nuclear power plants.^[1] The ferritic nozzle/coolant piping material is ASTM A508 Grade 3 Class I low-alloy steel and connecting piping material is SA312 Type 304LN austenitic stainless steel. This transition joint exhibits adequate strength and satisfactory resistance against intergranular stress corrosion cracking at operating condition.^[2] However, microstructure and chemical composition have been changed across fusion boundary for this type of weld. There are a number of factors responsible for these

changes: (i) different crystal structures between body-centered cubic (BCC) ferritic low-alloy steel and face-centered cubic (FCC) weld metal, (ii) cyclic thermal stress owing to difference in thermal expansion coefficient (CTE), (iii) diffusional mixing of alloying elements across fusion boundary, (iv) preferential oxidation at weld metal-ferritic steel interface (v) change of base metal dilution (BMD) affecting the composition gradient in weld metal, (vi) degeneration through creep in narrow carbon-denuded zone of ferritic steel, and (vii) phase transformation near fusion boundary.^[3] Initially, the common welding consumable was austenitic stainless steel and at latter stage Ni-base alloy has been used.^[4-6] Ni-base alloy has CTE in-between ferritic and austenitic steel with an additional advantage of restricting carbon diffusion. Carbon has low diffusivity in FCC nickel.^[7] Jang *et al.*^[1] have attempted to join low-alloy steel with 316 SS using IN 82 buttering material and IN 182 weld metal. Microstructural investigation revealed that fusion zone contained dendritic morphology with varying arm spacing, recrystallized structure, segregation, and secondary precipitation. Tensile properties were different across the fusion boundary of low-alloy steel and buttering material. Failure occurred through ductile dimple fracture during tensile testing. In a different endeavor, Alloy 800 low carbon steel was joined with 316LN SS using four types of weld metal *i.e.*, 316 SS, 16-8-2 SS, IN 182, and IN 82.^[6] With the use of 316 SS electrode, well-defined dendritic structure was developed. The transition

M. GHOSH, Senior Scientist, is with the Structural Characterization Group, MST Division, CSIR_National Metallurgical Laboratory, Jamshedpur 831007, India. Contact e-mail: ghosh_mnk@yahoo.com R. SANTOSH, Research Fellow, is with the Department of Mechanical & Manufacturing Engineering, Manipal Institute of Technology, Manipal 576104, India. S.K. DAS, Principal Scientist, G. DAS, Sr. Principal Scientist, and B. MAHATO, Tech. Officer, are with the Materials Science & Technology Division, CSIR_National Metallurgical Laboratory, Jamshedpur 831007, India, J. KORODY, Professor, is with the Department of Mechanical & Manufacturing Engineering, Manipal Institute of Technology, S. KUMAR, Scientific Officer, and P.K. SINGH, Scientific Officer 'G', are with the Reactor Safety Division, Bhaba Atomic Research Centre, Mumbai 400085, India.

Manuscript submitted December 9, 2014.

Article published online May 5, 2015

region with Alloy 800 exhibited unmixed zone and grain boundary liquation. After solidification, weld metal contained cellular structure when 16-8-2 SS filler alloy was used. Weld structure was austenitic with some amount of ferrite near fusion boundary when filler alloy was 316LN SS. Welded joints with IN 82 and IN 182 revealed signature of recrystallization along with grain boundary migration. Microhardness distribution exhibited increment in value adjacent to weld centerline due to carbon enrichment of weld metal. Transverse tensile testing revealed failure through fusion zone for joints with 316 SS and 16-8-2 SS weld metal and parent material failure for Ni-base alloys. At room temperature and 823 K (550 °C), UTS and YS of joints made with Ni-base weld metal showed superior strength with respect to joints fabricated with 316 SS and 16-8-2 SS weld metals. Another group of researchers established that microstructural variation near transition zone was governed by carbon content, cooling rate, and segregation of alloying elements.^[4,8] Welded specimens consisting of St37-2 carbon steel and AISI 304 SS using 8.5Ni-19.2Cr austenitic weld metal showed microstructural heterogeneity.^[4] Decarburized region and heat-affected zone with variable grain size were observed at steel side. In weld metal, primary austenite with small amount of eutectic ferrite was found. Partial recrystallization with small quantity of carbide precipitation occurred near the fusion boundary of parent austenitic steel.^[4] Tensile strength was ~400 MPa with 60 pct elongation. The hardness of weld zone exhibited substantial improvement (220-275 VHN) with respect to base materials. In this context, compatibility of Ni-base alloys and stainless steel was also examined.^[9-11] Hosseini and his co-workers^[9] have joined IN 617 with 310 SS using IN 617, IN 82, and 310 SS weld metals. With the use of IN 82, weld metal microstructure contained migrated grain boundary, solidification grain boundary, and Nb carbide precipitates. For IN 617 weld metal, the microstructure consisted of austenite with dendritic morphology and small amount of segregated Mo. 310 SS weld metal promoted to form both cellular and dendritic microstructure. The interface between IN 82 and IN 617 base metal exhibited unmixed zone. The fusion boundary between IN 617 and 310 SS revealed columnar growth with adequate mixing. Minimum bond strength was obtained for joints with IN 82 weld metal, where as bond strength was enhanced for assembly with 310 SS weld metal. Failure occurred through HAZ of 310 SS. In another endeavor, IN 657 was welded with 310 SS using IN 82, IN A, IN 617, and 310 SS weld metals.^[5] Region adjacent to fusion boundary of IN 617 and 82 contained unmixed, intermediate mixed, and hard zones. Highest strength was achieved for the weld fabricated with IN A weld metal.

Besides the use of austenitic stainless steel and Ni-base alloys as weld metal/buttering material, a number of failure incidents have been reported in recent past for dissimilar weld consisting of ferritic and austenitic steels.^[1,6] One of the failure modes was lack of fusion or disbonding at the vicinity of fusion boundary of ferritic steel.^[12] Another frequently occurred problem was wall cracking of IN 82/182 weld in hot leg nozzle causing leaking of primary water into containment.^[1]

The actual reasons for these incidents were yet to be confirmed. Some possible reasons were carbon imbalance across fusion boundary of ferritic steel-buttering material, formation of Type-II boundary, appearance of brittle phase near fusion boundary, and carbide precipitation in diffusion zone.^[3,13] Scope of the present investigation is a) carrying out detailed structural characterization of transition joint consisting of ferritic and austenitic steels with different buttering materials, b) assigning the weakest zone which becomes prone to failure during service, and c) confirming the preferable buttering material from the point of joint efficiency.

II. EXPERIMENTAL

A. Base Materials, Welding Consumables, and Welding

Base materials in the present study were SA508 Gr.3 Cl.I ferritic steel (hence forth low-alloy steel/LAS) and SA312 Type 304LN austenitic stainless steel (hence forth 304LN SS). Buttering materials were austenitic stainless steel (309L SS) and nickel-base alloy (IN 182). Weld metals were austenitic stainless steel (308L SS) and Ni-base alloy (IN 182), respectively. After layer wise buttering with ultimate thickness ~2-5 mm, post weld heat treatment was done at ~923 K (650 °C) to release stress. Chemical composition of these undiluted consumables and solution annealed base materials is furnished in Table I. Detailed welding technique was discussed elsewhere.^[14,15] Schematic of weld joint has been shown in Figure 1(a).

B. Sampling, its Preparation and Microscopy

From welded joints, sampling has been done from middle of transverse section and prepared by conventional metallographic technique. Sampling location is shown in Figure 1(b) with different numbers for various regions. Low-alloy steel was etched with 3 vol pct Nital and buttering material-weld metal-304LN SS were etched with Glycergia (mixture of HNO₃ and HCl ~1:3 with few drops of Glycerin). Microstructure of base alloys, fusion boundaries, buttering material, and weld metal was examined in optical microscope (OM, Leica). Finer structural details near fusion boundary of LAS and buttering material were explored in scanning electron microscope (FEI Nova Nano SEM) using secondary electron mode. Quantification and statistical analyses of microstructural features were performed using image analysis software.

C. X-ray Diffraction Study

X-ray diffraction (Bruker D8 Discover) was carried out near the fusion boundary between LAS and buttering material to identify the reaction products. Sampling was done by cutting a section parallel to fusion boundary by electric discharge machine. The cut surface was within low-alloy steel and was ~2.0 mm away from fusion line. The surface was polished and cleaned by sonication using acetone. Over that surface X-ray diffraction was performed. This technique was repeated by removing layer

Table I. Chemical Composition of Base Metals and Welding Consumables

Alloys	Concentration of Alloying Elements (wt pct)												
	C	Mn	P	S	Si	Ni	Cr	Mo	Cu	Al	N	Nb	Fe
Low-alloy steel	0.20	1.2	0.01	0.001	0.001	0.80	0.20	0.50	0.03	0.04	—	—	bal
304LN SS	0.03	2.0	0.05	0.03	1.0	8.0	18.0	—	—	—	0.1	—	bal
309L SS	0.03	1.0	0.03	0.03	0.65	12.0	23.0	0.75	—	—	—	—	bal
308L SS	0.03	2.0	0.05	0.03	1.0	10.0	19.0	—	—	—	—	—	bal
IN 182	0.10	5.0	0.03	0.02	1.0	bal	13.0	—	0.50	—	—	1.0	10.0

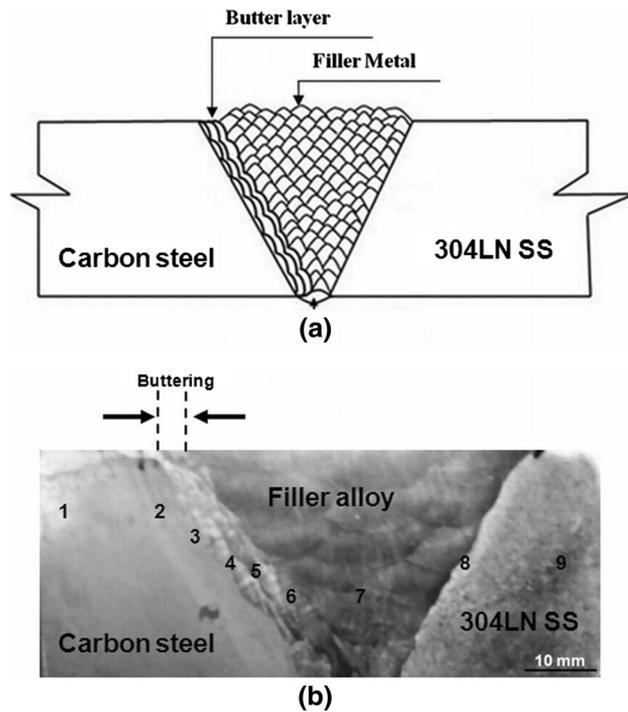


Fig. 1—Dissimilar metals welded joint (a) schematic diagram (not to scale) and (b) macro-image showing location of microstructural examination.

after layer so far the pure buttering material was reached. During X-ray diffraction study, the target was Cu, scanning span was 25-100 deg, step size was 0.02 deg/second, and residence time was 2 seconds. The phases were identified by peak matching using standard handbook (Powder Diffraction File, Version IV).

D. Evaluation of Microhardness

Microhardness was determined (Leica VHMT) across fusion boundaries at a depth of ~10 mm from top edge of weld. Microhardness was taken at an interval of ~1.0 mm using 50 g load and 15 seconds dwelling time. Near fusion boundary the interval was reduced to 0.3 mm for identifying drastic change over a narrow region.

E. In Situ Deformation and Fractography

In the published literature, it was reported that premature failure/disbonding of this type of joints

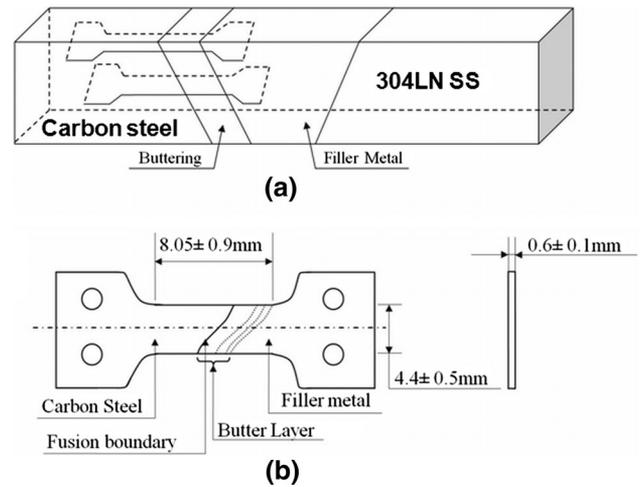


Fig. 2—Tensile specimens from dissimilar weld (a) location and (b) schematic drawing of prepared sample (not to scale).

occurred pre-dominantly from interface close to low-alloy steel.^[1,4,6,16-18] Therefore, in this study, sampling has been carried out close to the center of transverse section (~10 mm from top edge of welded specimen) through low-alloy steel-buttering material interface as shown in Figure 2(a). Fusion boundary between low-alloy steel and buttering material was nearly at the center of gage length. The machined specimen has been shown in Figure 2(b). Experiments have been done in deformation stage with 1 kN load cell, attached to SEM (Hitachi 3400N). At each joining parameter, three samples were tested. Cross head speed during tensile testing was ~0.05 mm/min and data acquisition rate was ~500/second. Before testing, one of the surfaces of rectangular specimen was polished by conventional metallographic practice. At regular interval, snap shot was taken to study the microstructural change over gage length. After testing, one of the fracture surfaces was studied in SEM to reveal the specific characteristics.

III. RESULTS

A. Microstructural Investigation

Microstructures of low-alloy steel and 304LN SS (location 1 and 9, respectively) are shown in Figures 3(a) and (b). LAS exhibited tempered martensitic structure and the presence of prior austenitic grain boundary

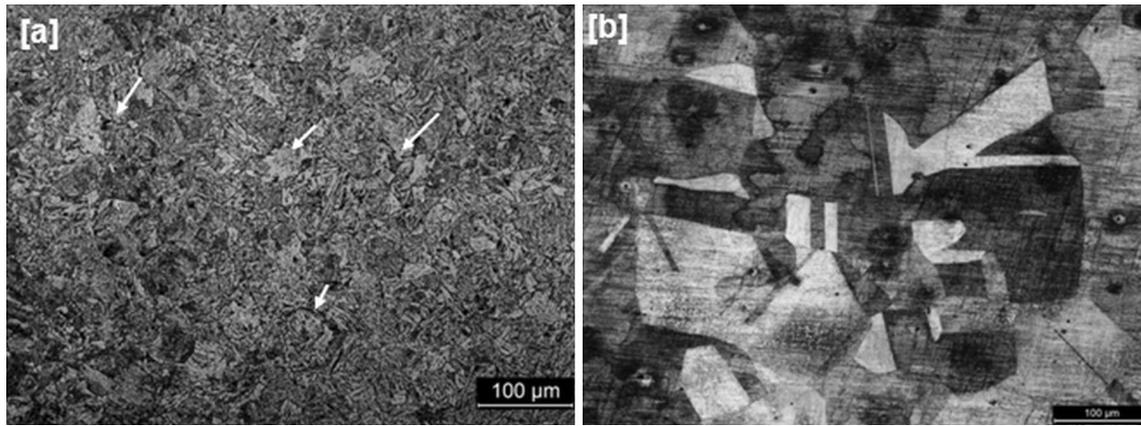


Fig. 3—Base material microstructure (a) low-alloy steel and (b) 304LN SS.

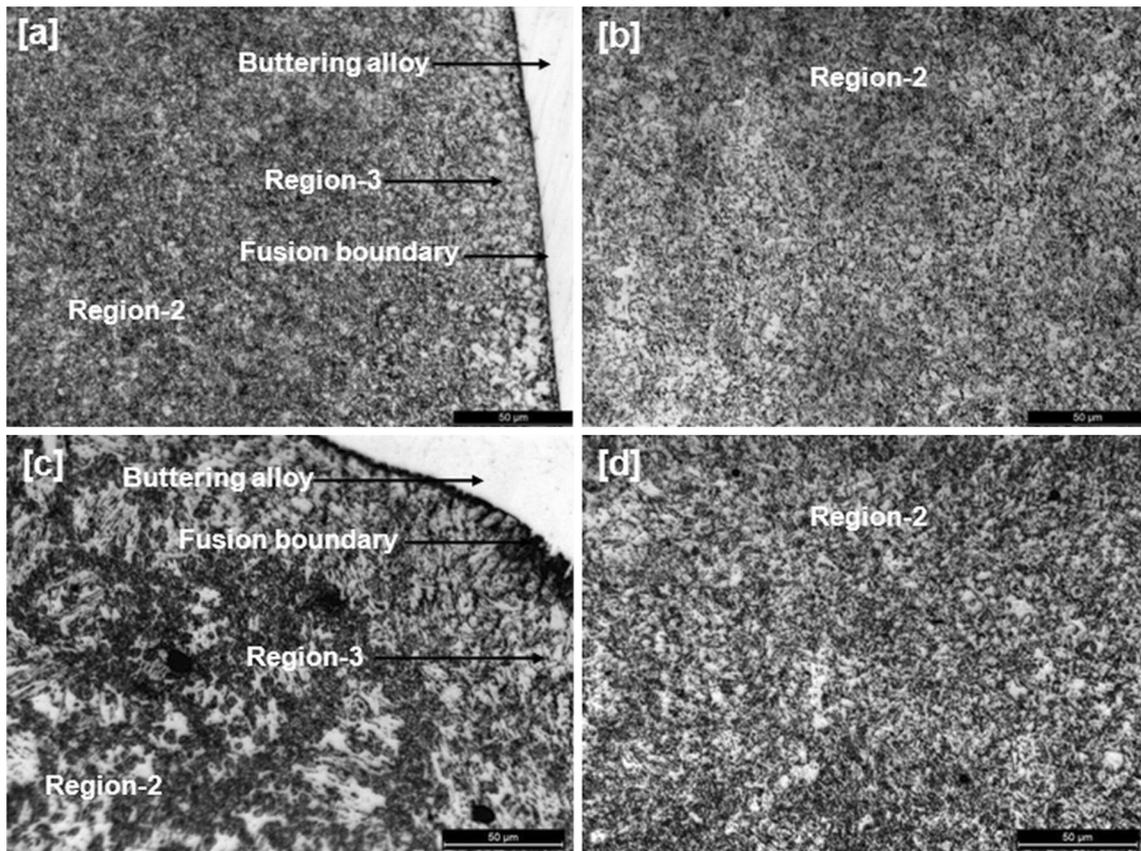


Fig. 4—Optical micrographs of welded joints (a) and (b) buttering with 309L SS, (c) and (d) buttering with IN 182. Images exhibited phase distribution at different regions of low-alloy steel.

(white arrows in Figure 3(a)). 304LN SS contained polygonal grains with occasional appearance of twins.

Microstructure of low-alloy steel after welding could be divided into three regions: Region-1, Region-2, and Region-3 (Figure 1(b)). Region-1 corresponded to base material. Region-2 exhibited fine polygonal ferrite grains containing pearlite at grain boundary/grain boundary triple point (Figures 4(b) and (d)). Adjacent to fusion line (Region-3), the area contained ferrite-pearlite phase mixture and ferrite grains were coarse (Figures 4(a) and

(c)). Depending on buttering material and welding technique, there was a variation in the width of these regions and ferrite grain size (Table II). Regions 4-6 of buttering material exhibited solidification microstructure. Both 309L SS and IN 182 buttering materials consisted of dendritic structure. Packets of austenite/ferrite (AF) solidification characteristic were observed for 309L SS buttering material at some locations (Figure 5(a)). Buttering with IN 182 exhibited recrystallization accompanied by grain boundary migration

Table II. Width of Various Regions in Different Welds

Sample ID	Low-Alloy Steel Side (μm)		Butter Material (μm) Region 4 + 5 + 6
	Region-3	Region-2	
309L buttering (WL 309)	15 to 36	350 to 1000	2500 to 4500
IN 182 buttering (WL182)	37 to 55	900 to 1200	2000 to 5500

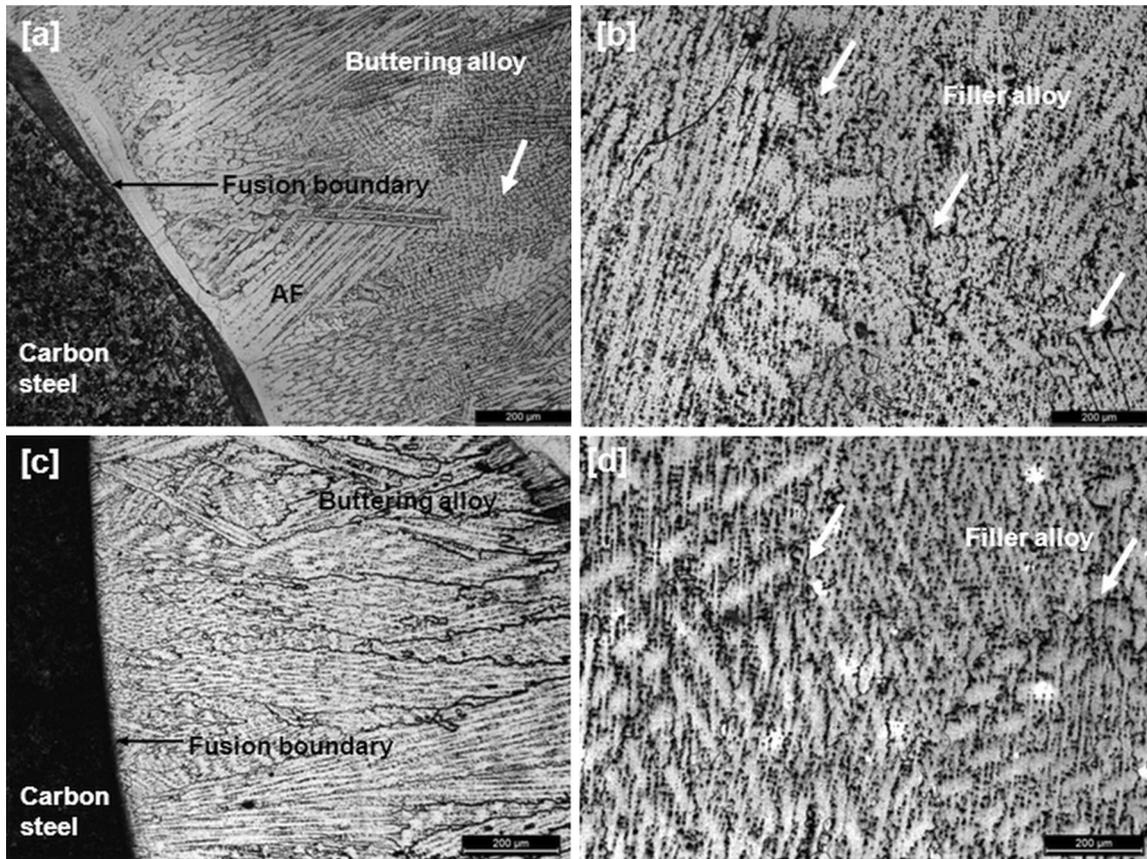


Fig. 5—Optical images of welded joints (a)–(b) buttering with 309L SS and (c)–(d) buttering with IN 182.

(Figure 5(c)). The boundary between buttering material and weld metal illustrated limited mixing with each other. Cellular structure and solidification boundaries were observed within weld metal (Figures 5(b) and (d)). Fusion boundary between weld metal and 304LN SS was nearly straight (Figure 6). Grain growth was perceived for 304LN SS and epitaxial growth was found within weld metal adjacent to fusion boundary (Figure 6).

For both welds adjacent to fusion boundary of low-alloy steel and buttering material, two different boundaries were present—one was perpendicular to the fusion boundary, known as Type-I boundary and the other was parallel to fusion boundary, termed as Type-II boundary (Figure 7). Close to fusion boundary, blocky islands of irregular geometry were found. This area contained fine lath of martensite as depicted in SEM-SE images (Figure 8). The distribution of martensite cluster was heterogeneous in nature.

B. Microhardness Evaluation

Microhardness profiles at two fusion boundaries for the welds are given in Figure 9. Near low-alloy steel-buttering material interface, a peak was observed which was much higher than that of parent phases (Figures 9(a) and (b)). It corresponded to the formation of martensite. In low-alloy steel immediately after peak hardness, there was a decrease in microhardness and attributed to the presence of region-2 and region-3. Further movement toward LAS showed increment in hardness due to the presence of tempered martensite (~275 VHN). Within buttering material, there was decrement in microhardness after the peak, indicating softening. Away from fusion boundary, little upward trend in profile was identified and finally it maintained a steady state within weld metal. Microhardness profile near the fusion boundary of weld metal and 304LN SS showed slight increase (~290 VHN) with respect to both alloys (Figures 9(c) and (d)). The increment was nearly same for both the joints.

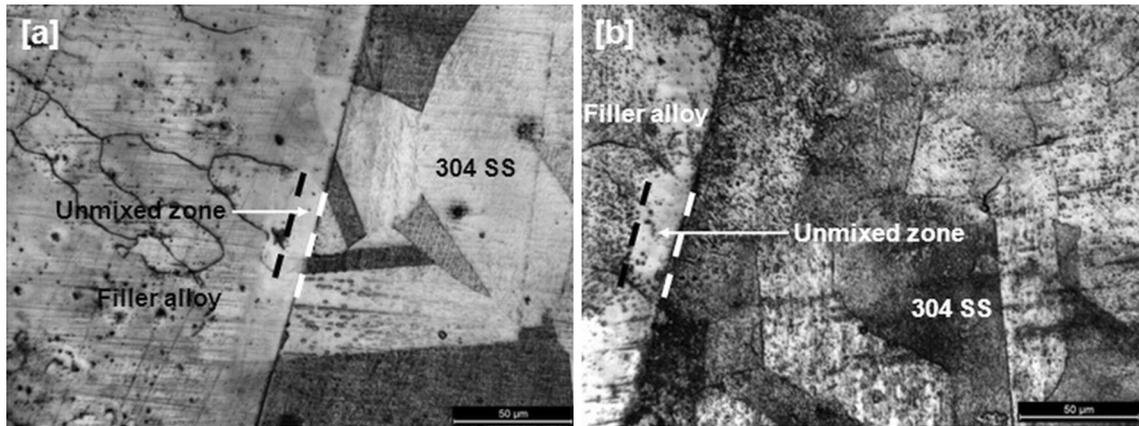


Fig. 6—Optical micrographs near fusion boundary of welds; buttering with (a) 309L SS and (b) IN 182. Figure showed weld metal—304LN SS interface.

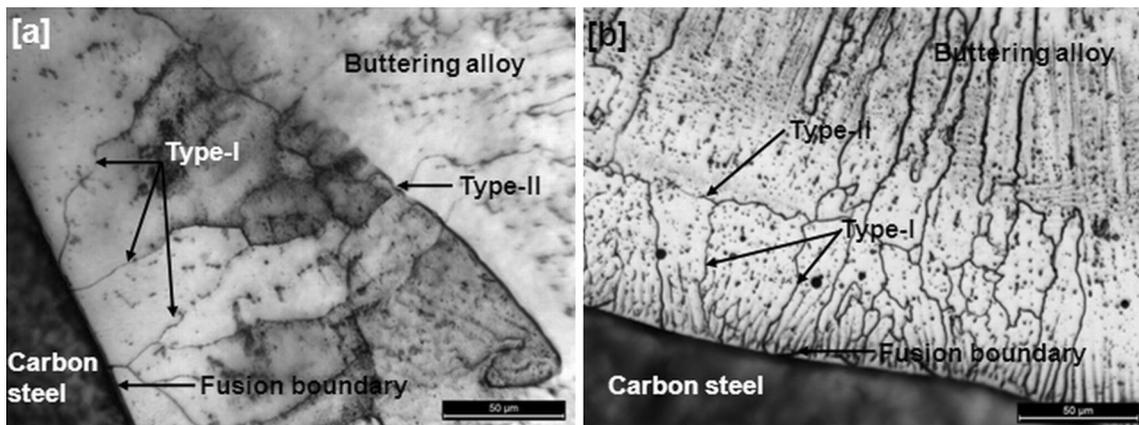


Fig. 7—Optical images of welded joints buttering with (a) 309L SS and (b) IN 182. Figure revealed Type-I & Type-II boundaries.

C. X-ray Diffraction Study

The characteristic X-ray spectrum of area near fusion boundary of low-alloy steel and buttering material is shown in Figure 10. Both the joints revealed martensite formation within austenitic buttering material. Apart from these two phases, no other phase formation, like carbide *etc.*, was identified.

D. In Situ Tensile Testing

Two representative graphs of tensile testing are shown in Figure 11. Flat portion of the graph at initial stage (~3 pct strain) was owing to grip adjustment. Yield strength and ultimate tensile strength were found higher for WL 309 than that of WL 182 (Table IV). Change in buttering material has marginal effect on ductility of joints. During deformation, SEM-SE images were captured to explore structural changes (Figure 12). Before yield point, no such notable change was observed. The shear bands appeared when the sample crossed the limit of yield stress (black arrows in Figure 12). Near fusion boundary, the shear bands were parallel (Figures 12(a) and (c)) to loading axis (*i.e.*, perpendicular to fusion

boundary). Away from fusion boundary, the orientation of shear bands was changed from grain to grain (Figures 13(a) and (b)). Deformation was confined within buttering material. Crack initiated from edge over gage length, moved nearly parallel to fusion boundary, and was within the buttering material. Failure occurred in ductile mode for both assemblies through micro-void coalescence (Figures 14(a) and (b)).

IV. DISCUSSION

Microstructure of welded assemblies was complex along transverse section. It contained four different materials and three interfaces. Close to fusion boundary (region-3), the microstructure of low-alloy steel consisted of large polygonal ferrite grains with shaded ill-defined pearlite (~5 pct). Decarburization occurred in this narrow band.^[4] Ferrite grains were coarser in comparison to adjacent region-2. Partial melting followed by re-solidification during welding and subsequent post weld heat treatment promoted carbon migration from region-3 to buttering material due to concentration gradient.^[3] A Coarse deeply etched zone

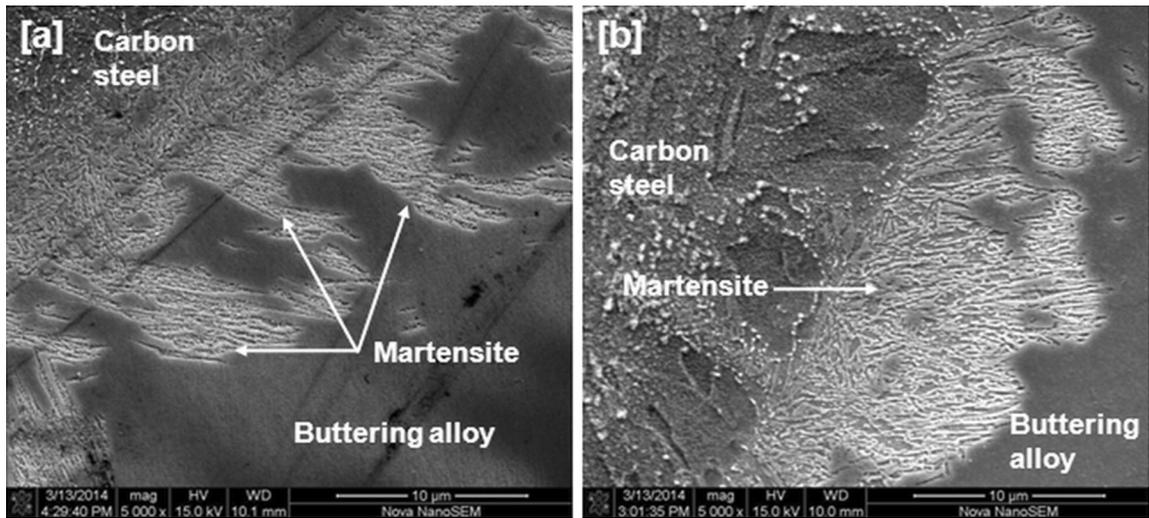


Fig. 8—SEM secondary electron images of welded assemblies; buttering with (a) 309L SS and (b) IN 182. Figure illustrated the presence of fine lath martensite.

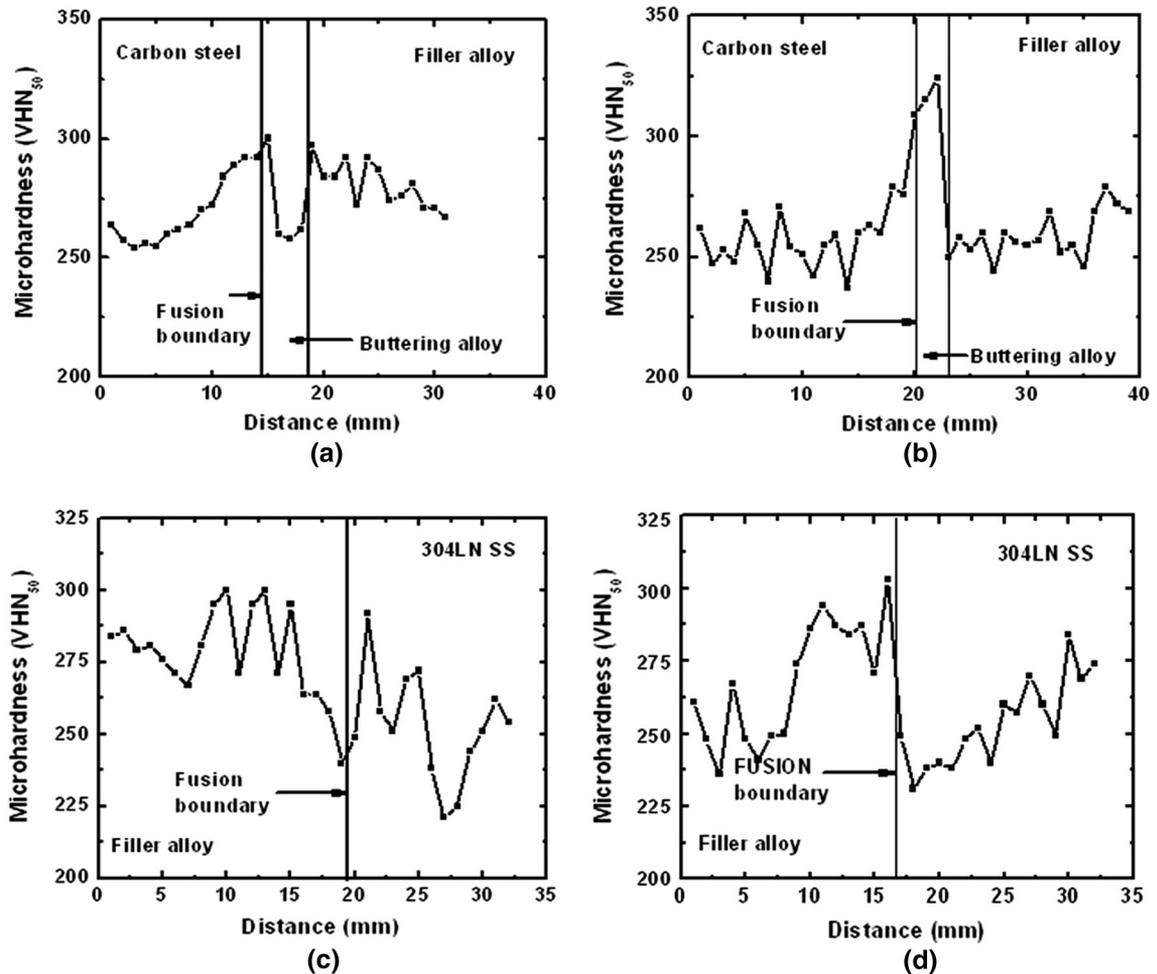


Fig. 9—Microhardness profile of welded assemblies (a) and (c) buttering with 309L SS, (b) and (d) buttering with IN 182.

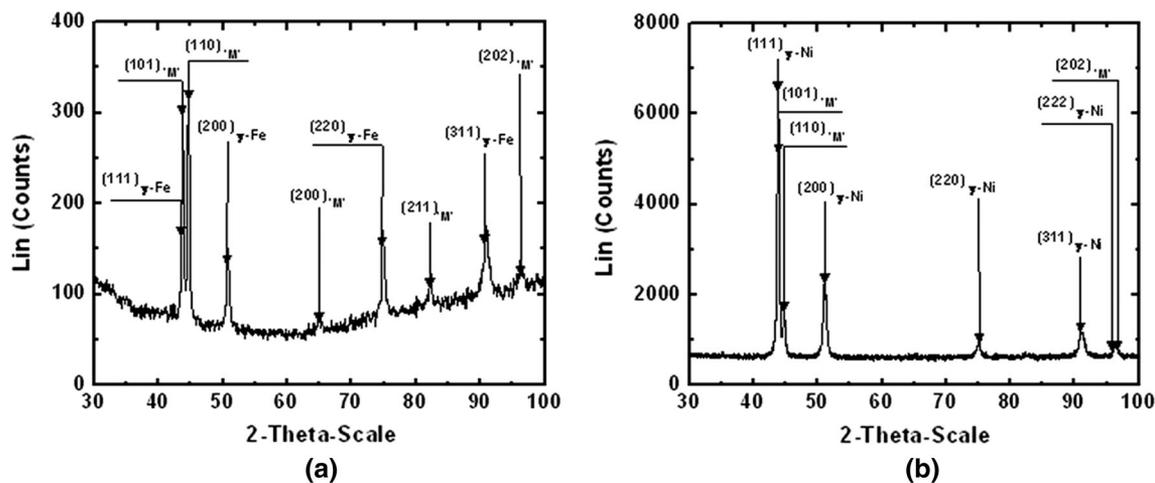


Fig. 10—Characteristic X-ray spectrum close to fusion boundary of low-alloy steel-buttering material (a) buttering with 309L SS and (b) buttering with IN 182.

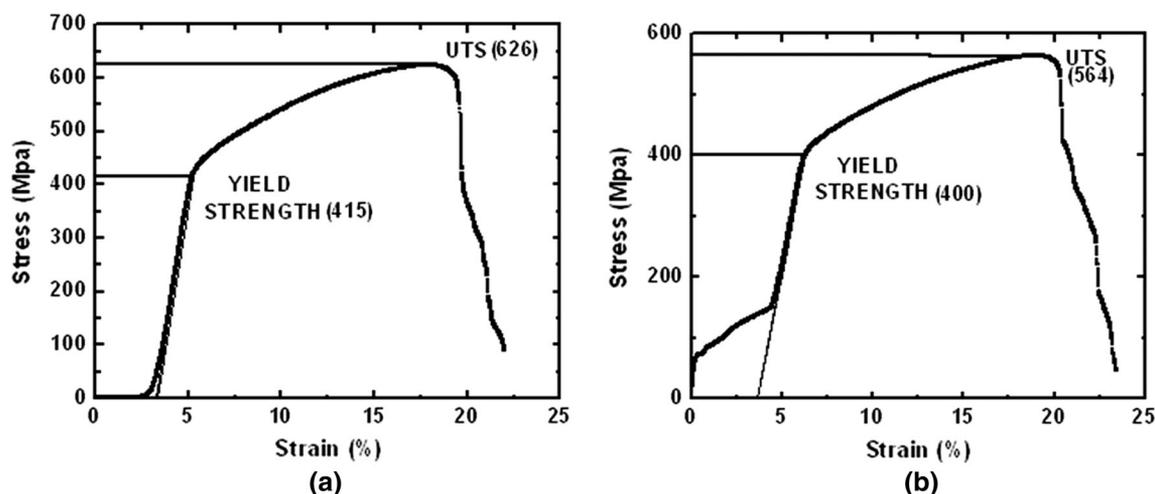


Fig. 11—Engineering stress-strain diagram of welded assemblies obtained during *in situ* deformation (a) buttering with 309L SS and (b) buttering with IN 182.

near interface of ferritic side was reported by Celik *et al.*^[4] during welding of St37-2 and AISI 304 steels using 8.5Ni-19.2Cr weld metal. They found carbon concentration of this region was lower than the bulk and termed the region as decarburized band. Carbon deficiency impelled decrease in second phase area fraction with respect to region-2. Pinning effect on ferrite grain boundary by second phase was reduced and grain size of ferrite was increased.^[19] Grain size of this region was $\sim 12 \mu\text{m}$ for both welds. The width of coarse grain region was more for WL 182 in comparison to WL 309 (Table II). The former joint was produced through SMAW and the latter one by GTAW.^[14,15] SMAW provided higher heat input with respect to GTAW.^[20] In region-2, the original microstructure of parent alloy was disappeared and consisted of ferrite + pearlite phase aggregate. This region experienced heat dissipation after welding and heat input during post weld heat treatment. Partially tempered martensite was transformed to stable ferrite + pearlite microstructure. Matrix grain growth

was restricted owing to the presence of sufficient quantity of pearlite (~ 10 pct). Matrix grain size of this region was nearly same for both welds. However, owing to difference in heat input, the width of region-2 was larger for WL 182 with respect to WL 309 (Table II).

The solidification microstructure in austenitic buttering material was pre-dominantly dendritic in nature.^[4] IN 182 contained substantial amount of Fe and Nb as alloying elements. Iron reduced Nb solubility in Ni-Cr austenitic solid solution.^[21] Nb migrated toward interdendritic region and encouraged segregation and constitutional supercooling.^[22] This constitutional supercooling promoted epitaxial growth with predominant dendritic morphology as shown in Figure 5(c).^[9,22] Nb partitioning in inter-dendritic region was observed by Naffakh and his co-workers for DMW between AISI 310 SS and IN 657.^[5] They pointed out that it might lead to embrittlement to the assembly. Nb-enriched carbide precipitation could be also expected in inter-dendritic regions owing to drop in equilibrium distribution

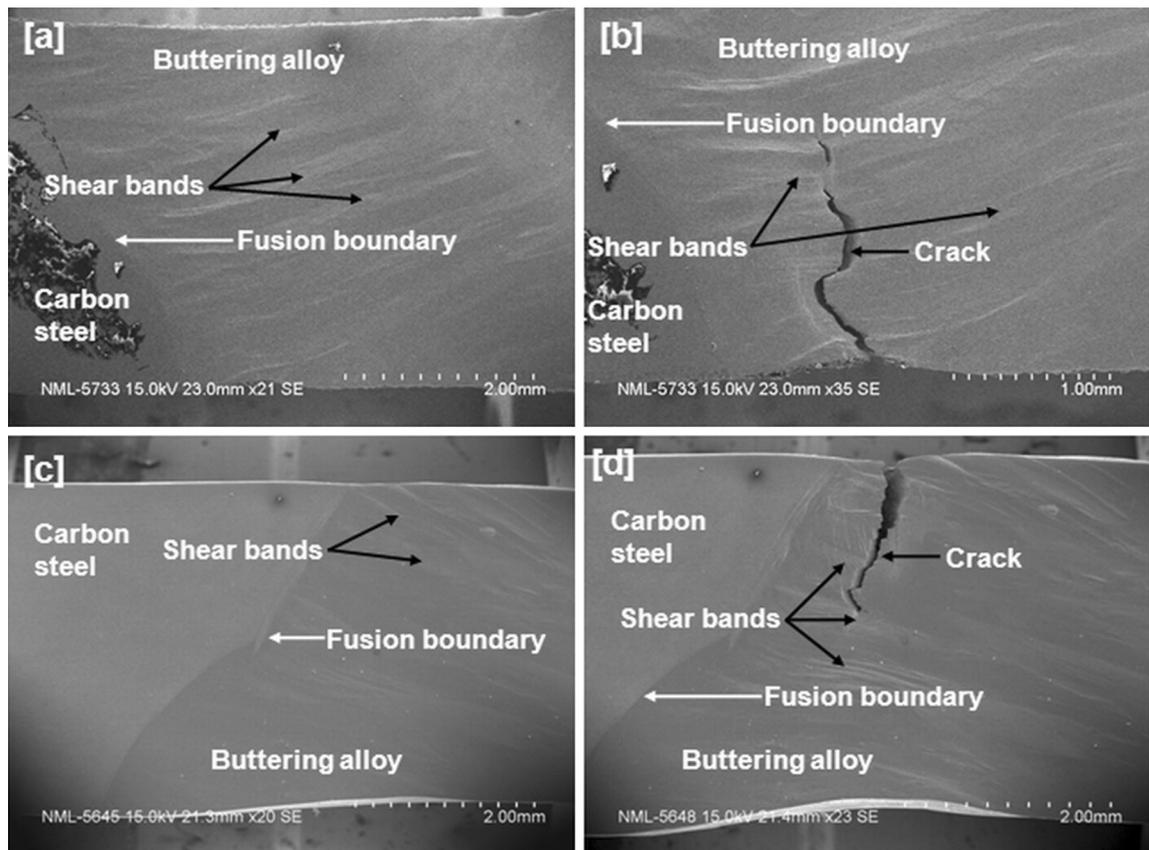


Fig. 12—SEM secondary electron images during *in situ* deformation of welded joints (a) buttering with 309L SS exhibiting shear band formation just above YS, (b) buttering with 309L SS showing crack propagation from edge, (c) buttering with IN 182 revealing shear band appearance above YS and (d) buttering with IN 182 illustrating fracture initiation from edge.

co-efficient of the same element below unity.^[9] Buttering material 309L SS after solidification exhibited columnar dendrites. During welding dilution of buttering material was increased due to iron migration from low-alloy steel. Iron enrichment in buttering material decreased Mo partitioning co-efficient.^[5] This resulted in Mo constitutional under cooling to promote columnar morphology.^[23] The effect of Mo during solidification was discussed in details by Naffakh *et al.*^[5] to explain the coarse and thin dendritic structure of weld metal. They found that nature of dendritic morphology was controlled by relative concentration of Fe and Mo in weld metal during producing dissimilar welds with different Ni-base alloys. Solidification primarily occurred in austenitic mode with co-existence of austenite/ferrite at localized regions (Figure 5(a)). A part of the dendritic structure contained fine-equiaxed morphology also (arrow in Figure 5(a)). A lower heat input to this region for WL 309 with respect to WL 182 resulted in higher cooling rate to develop fine microstructure. The fine microstructure on the other hand has lower tendency of Mo segregation.^[5,21] Migrated grain boundary as found in Figure 5(c) is nearly absent in Figure 5(a). The reason might be the precipitation of large amount of alloy carbide along solidification front to pin grain boundary.^[9]

After solidification, weld metal consisted of primary austenite with cell morphology. Major chemical species

in weld metal were Ni and Cr. They have negligible tendency for segregation.^[9] Therefore, constitutional supercooling was absent and cellular morphology was produced for both welds under minimum driving force. Large quantity of secondary phases, oxide inclusions, and globular precipitates was observed. The presence of secondary phases, precipitates, and inclusions in solidified austenitic stainless steel weld metal was also reported for DMW between 310 SS and IN 657.^[5] Grain boundary migration was noticed in weld metal, which cut through solidification structure (arrow in Figures 5(b) and (d)).

Out of three interfaces, first one was between low-alloy steel and buttering material. Type-I boundary was found for both welds in buttering material (Table III). They originated from fusion boundary. This boundary appeared when columnar grain growth of parent material took place in buttering material and became nearly perpendicular to fusion boundary.^[9,12] Type-II boundary was observed within few micron distances from fusion boundary (Table III). They formed as a planar interface when low-alloy steel was austenite.^[3] Near melting point LAS was ferritic (delta ferrite) and the buttering material was austenitic. In that situation normal epitaxial growth was forbidden and heterogeneous nucleation of fcc buttering material was occurred.^[5,12,24,25] This resulted in Type-II boundary parallel to fusion boundary.^[12] The mechanism of

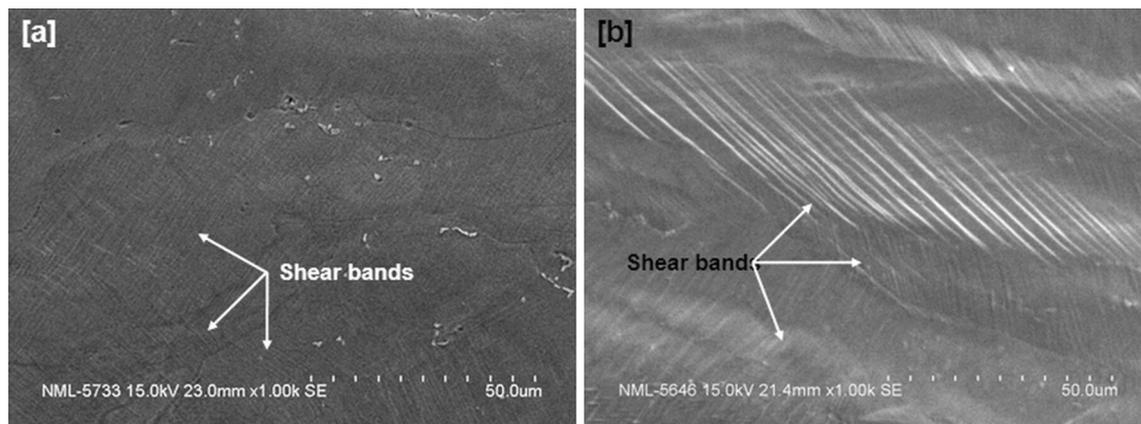


Fig. 13—Images were taken in SEM-SE mode during *in situ* deformation and exhibited change in orientation of shear bands from one grain to other within buttering alloy (a) with 309L SS and (b) with IN 182.

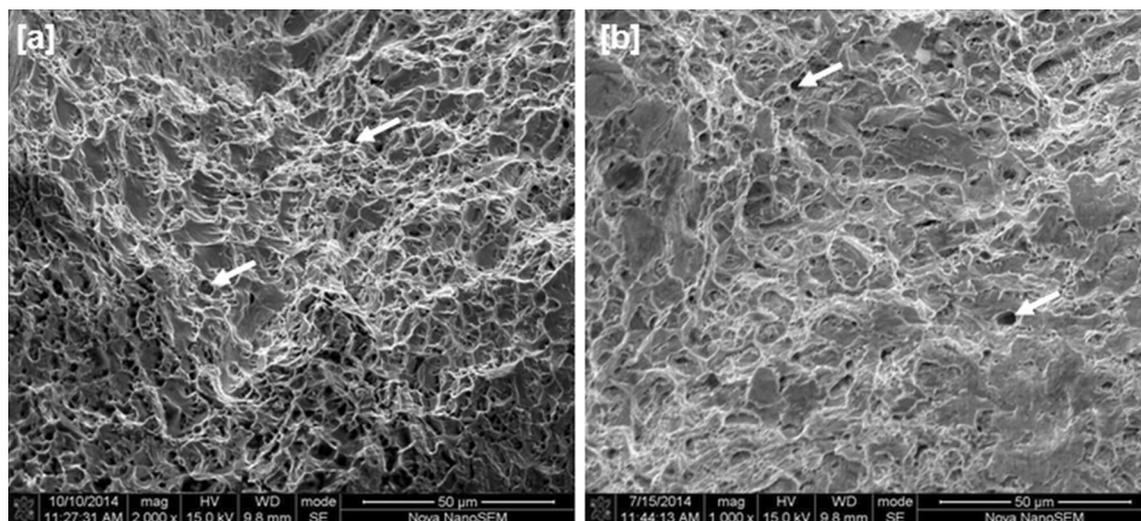


Fig. 14—Fractographs of samples after *in situ* tensile testing (a) buttering with 309L SS and (b) buttering with IN 182.

Table III. Quantified Microstructural Features of Different Regions

Sample ID	Ferrite Grain Size at Low-Alloy Steel Side (μm)		Distance of Type-II Boundary from Fusion Boundary (μm)	Martensite Layer Thickness (μm)
	Region-2	Region-3		
WL 309	5.7 ± 0.8	12.5 ± 0.5	13 to 18	7 to 16
WL 182	7.1 ± 0.4	11.8 ± 0.8	12 to 44	2 to 10

formation and nature of Type-II boundary were discussed elaborately by DuPont *et al.*^[3] Type-II grain boundary was characterized for ferritic alloy clad with austenitic steel and Monel-iron system.^[26,27] Essentially in both cases, it was ferrite-austenite combination at welding temperature. It has been illustrated that Type-II boundary could not form if base material and buttering material were of same composition/crystal structure. With the progress of solidification, the interface was changed from bcc-fcc to fcc-fcc with orientation mismatch. However, both alloys consisted of same

crystal structure and driving force developed by temperature-composition-strain gradient kept the boundary mobile until its movement was ceased by drop in temperature.

At the same interface phase transformation occurred. Alloying elements diffused due to the concentration gradient across fusion boundary. Low-alloy steel contained higher amount of carbon than that of buttering material. Therefore, carbon migrated toward buttering material during welding as well as post weld heat treatment from LAS.^[3] Both 309L SS and IN 182

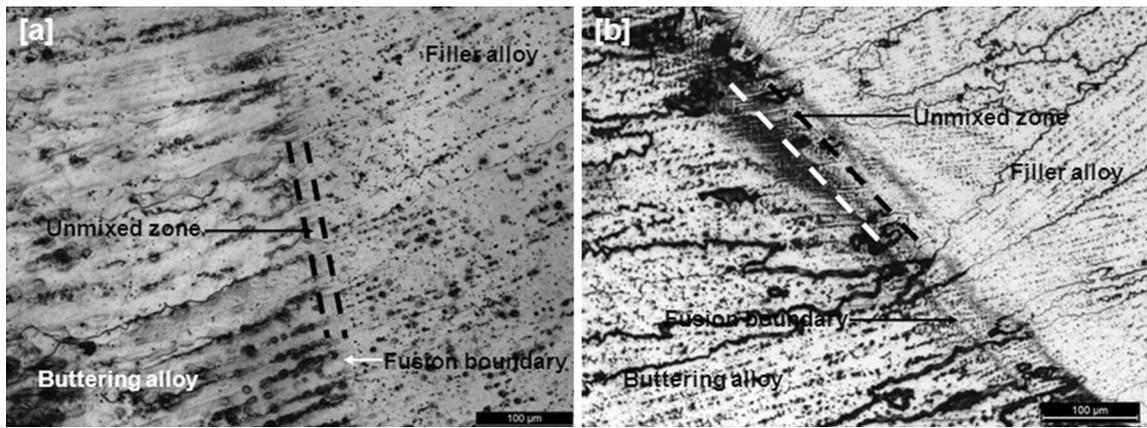


Fig. 15—Optical photographs of buttering material-weld metal interface; buttering with (a) 309L SS and (b) IN 182.

Table IV. Tensile Properties of Welds at Room Temperature During *In Situ* Deformation

Sample ID	0.2 pct Off Set Yield (MPa)	Ultimate Tensile Strength (MPa)	Ductility (pct)
WL 309	418 ± 4	643 ± 12	16 ± 1
WL 182	379 ± 8	584 ± 10	17 ± 1

buttering materials contained high amount of Cr and the same element was nearly absent in low-alloy steel. This local heterogeneity has a catalytic effect for carbon migration during post weld stress relieving.^[28] Carbon migration thus increased the carbon equivalent locally in buttering material side adjacent to fusion boundary and shifted the TTT diagram toward right.^[29] In that case relatively slow cooling rate, *i.e.*, air cooling, propelled martensite transformation.^[30] This resulted in appearance of narrow martensitic band close to the fusion boundary (Table III).^[31] Martensitic islands were well within the Type-II boundary. Being a hard phase, the presence of martensite created strain in adjacent region. This was responsible for increment in hardness. Martensite that was formed during welding became tempered during post weld heat treatment. At the same time, new martensitic lath was also appeared during cooling after post weld heat treatment. The obtained microhardness was the synergistic effect of both of these two types. Martensite formation was confirmed by X-ray diffraction study (Figure 10). The width of martensitic layer was smaller for WL 182 in comparison to WL 309 owing to limited diffusion of carbon in former with respect to latter.^[13] Compositional gradient across fusion boundary has a predominant effect on martensite start temperature (M_s) and width of martensitic zone.^[3] At the time of using Ni-base alloy as buttering material, concentration gradient in transition zone became large, this stabilized austenite in shorter region to promote thin width martensitic zone.^[3] The non-uniform width/discontinuous presence of martensitic region in both welds might be attributed to local variation in composition, fluid flow behavior, and cooling rate.^[3,13]

The second interface was between buttering material and weld metal. Unmixed zone was formed near interface (Figures 15(a) and (b)). This maintained a laminar morphology between two alloys along fusion

boundary and occurred when melting point of two alloys was close to each other.^[3] The occurrence of unmixed zone was reported by Sireesha *et al.*^[6] during welding of 316L SS and Alloy 800 using austenitic stainless steel and Ni-base alloys weld metals. This unmixed zone was also present for 310 SS, IN 617, and IN 82 weld metals during welding of IN617 with 310 SS.^[9] Limited extent of melting of substrate followed by re-solidification with minimum dilution resulted in un-mixed zone formation.^[5,6,27,28] The width of unmixed zone was close to each other as buttering material and weld metal were compatible to each other. The third interface was developed across the fusion boundary of weld metal and 304LN SS. At this interface, the unmixed zone of WL 182 exhibited larger width (~20-25 μm) than that of WL 309 (~12-15 μm). This was perhaps because of the incompatibility of IN182 with 304LN SS in comparison to 308L SS with 304LN SS. Adjacent to third interface, 304LN SS exhibited grain coarsening because of temperature rise during welding. Severe grain growth (~75 μm) was occurred for matrix grains of 304LN SS with respect to as-received base material (~55 μm).

Microhardness profile across the welded joints exhibited variation depending on phase evolution at different locations. Peak hardness was observed near the fusion boundary of low-alloy steel and buttering material due to the presence of martensite.^[3] Greater width of martensitic layer for WL 309 was endorsed by wider peak of maximum hardness with respect to WL 182 (Figures 9(a) and (b)). This trend envisaged higher extent of carbon diffusion in 309L SS in comparison to IN 182 during welding and post weld heat treatment.^[3,32] Immediately after peak, within buttering material microhardness was dropped. Average hardness of this region for WL 309 was ~255 VHN and that of WL 182 was ~240 VHN. Lower average trend in

microhardness of WL 182 can be attributed to lower inherent strength of IN 182 (UTS ~552 MPa) with respect to 309L SS (UTS ~575 MPa).^[33] As the profile entered in weld metal, the average microhardness was either increased to a small extent owing to high strength of 308L SS (UTS ~593 MPa) or followed a steady state (for IN 182). Average microhardness of region-2 of low-alloy steel exhibited a drop (~260 VHN) with respect to peak hardness. Further away from fusion boundary in LAS, the region consisted of mixed microstructure with lot of fluctuation and finally attained a steady state to show the hardness of parent alloy. The microhardness of region-3 was expected to be low owing to softening as discussed above.^[32] However, the value cannot be measured precisely because of its extremely thin width. The hardness value across austenitic region (weld metal and parent 304LN SS) was changed very little as temperature fluctuation during welding did not influence any phase transformation.^[4] It was reported that intergranular precipitation of chromium carbide occurred along with transgranular tiny δ -ferrite during welding.^[34] Confirmation of their presence was beyond the scope of present study. However, this phenomenon put a signature on the profile by exhibiting greater microhardness (~290 VHN) of this region with respect to adjacent regions.

To accommodate tensile samples on SEM stage, the gage length was restricted ~8 mm with first interface at center (Figure 2(b)). Thus, one-half of gage length contained region-3, region-2, and partially region-1 of low-alloy steel. On the other half of gage length, complete buttering material and partly weld metal were present. During testing, no deformation was recorded in low-alloy steel side as the average hardness of different regions of LAS was more than that of buttering material. Deformation started as the stress-strain curve crossed yield strength with the appearance of parallel shear bands. Shear bands were the collection of planar defects which formed during overlapping of stacking faults on closed packed planes of austenite during deformation.^[34] A number of shear bands were increased with the increment in strain and stress (Figures 12(b), (d), and 13). Near UTS, intersecting shear bands were appeared (Figure 13). Distance between two successive shear bands adjacent to fracture surface was higher for WL 309 (~0.5-1 μm) with respect to WL 182 (~0.1-0.4 μm). This finding might be attributed to higher stacking fault energy of Ni-base alloy (80-100 mj/m^2) with respect to austenitic stainless steel (~14-30 mj/m^2).^[14,35,36] Failure occurred from the weakest zone, *i.e.*, buttering material, as the minimum in microhardness profile was within this region. Bond strength was lower for WL 182 with respect to WL 309. Fracture surface was nearly parallel to fusion boundary; however, distance of fracture path from first interface was more for WL 309 (~0.8-2.0 mm) than that of WL 182 (~0.4-1.2 mm). Diffusional distance of alloying elements from low-alloy steel to 309L SS was more than the migrated distance of the same elements from LAS to IN 182. This characteristic promoted wider solid solution strengthened zone and kept the fracture path away from fusion boundary.

There are a number of reports on joint efficiency for dissimilar welds. Tensile tests on miniature samples were carried out for welded joints between carbon steel and F316 SS stainless steel. In that case IN 82 was buttering material and IN 182 was weld metal.^[1] Ultimate tensile and yield strength were ~503-545 and ~356-403 MPa depending on location of sampling. It was inferred that grain coarsening and sample thickness were mainly responsible for variation in strength. Celik and Al-saran^[4] studied the dissimilar weld between Alloy St37-2 and AISI 304 with weld metal 85Ni-19.2Cr stainless steel. They found that failure during tensile testing occurred at the interface between austenitic stainless steel and weld metal. This fact was attributed to low residual stress of AISI 304 with the capability of accommodating maximum plastic strain. Transition joints were fabricated between 310 SS and IN 657 using four different weld metals like IN 82, IN 617, IN A, and 310 SS.^[5] The investigation reported parent material failure for IN 657 owing to its inherent coarse and fully dendritic microstructure. Using IN A, the joints exhibited highest strength and total elongation. Joint made with IN 82 weld metal possessed lowest ultimate strength. Use of IN 617 weld metal for the same parent materials provided lowest total elongation. The welded joint between 316LN SS and Alloy 800 with four different weld metals like 316 SS, 16-8-2 SS, IN 182, and IN 82 revealed wide variation in mechanical properties.^[6] Highest strength was obtained for the assembly with IN 82 weld metal (~630 MPa). The lowest strength was found for the joint produced with 16-8-2 SS (~530 MPa) weld metal. Joints fabricated with 316 SS and 16-8-2 SS weld metals failed from the welded line. Transition joints prepared with IN 182 and IN 82 weld metals were broken from base material. Ductility of the joints was ~30-36 pct for Ni-base alloy and 25-26 pct for stainless steel weld metals. Evaluation of mechanical properties for weld consisting of low-alloy steel and 304LN stainless steel with IN 82 buttering material and IN 82/182 weld metal was attempted through ball indentation method.^[14] It was stated that UTS was close to parent stainless steel and HAZ exhibited higher strength than base material. Comparing published illustrations, present study revealed that welded joint with relatively cheaper buttering material, *i.e.*, stainless steel provided better joint efficiency than that of welded joint with buttering material IN 182 without compromising ductility.

Fractographs revealed dendritic morphology of that region where micro-voids were aligned along primary dendrites. Couple of voids contained dark irregular-shaped second phase/particles (Figure 14, white arrows). This indicated inter-dendritic coring with segregation to propel micro-void initiation. Change in fracture morphology with the change in buttering material was discussed by Shariatpanahi *et al.*^[37] They produced joints between 2.25Cr-1Mo ferritic steel and 316L austenitic stainless steel without and with 3-5 mm buttering material. Ductility of welded assembly was raised with the increment in thickness of buttering material, but joint efficiency was dropped. Fracture surfaces contained ductile tear ridges with numerous

interspersed dimples. The presence of buttering material changed the fracture mode from inter-dendritic to transdendritic. However, in present study, as collated in Table IV, variation in UTS of ~70 MPa did not bring about significant change in aspect ratio of dimples (~1.8) for two different welded joints.

V. CONCLUSIONS

Dissimilar metals welded joints were produced between low-alloy steel and 304LN stainless steel. Weld metal was 308L stainless steel and IN 182. Buttering was done with 309L stainless steel and IN 182, respectively. Detailed microstructural investigation was carried out. *In situ* deformation was performed to evaluate the mechanical properties of welds. Microhardness profile was obtained across the fusion boundaries to explore phase evolution at different regions and to identify weakest link in transition joint. Major observations are summarized below:

1. Low-alloy steel after welding consisted of two distinct microstructures, completely tempered fine grain polygonal ferrite-pearlite phase aggregate away from fusion boundary and coarse grain carbon-depleted ferrite-pearlite phase mixture adjacent to fusion boundary. Matrix grain size of these two regions was independent of nature of buttering material.
2. Adjacent to fusion boundary of low-alloy steel and buttering material, microstructure was heterogeneous. It contained discontinuous Type-I and Type-II boundaries along with clusters of fine lath martensite. The presence of martensite was confirmed through microhardness evaluation and X-ray diffraction study. The average width of martensitic cluster was more for WL 309 comparing to WL 182 owing to enhanced diffusional effect of alloying elements from LAS toward buttering material in case of former with respect to latter.
3. The interfaces between buttering material—weld metal and weld metal—304LN SS exhibited unmixed zone with variable width. Adjacent to weld metal—304LN SS, the matrix grain size of parent stainless steel was enhanced due to thermal effect.
4. Solidification microstructure of weld metal consisted of cellular morphology with the presence of primary austenite. Oxide inclusions and globular precipitates were present in matrix.
5. The microstructure of buttering material was predominantly dendritic. Constitutional supercooling in case of IN 182 promoted epitaxial growth. On the other hand, buttering with 309L SS demonstrated columnar dendrites owing to reduced Mo partitioning co-efficient. A part of dendritic morphology possessed fine-equiaxed structure because of high cooling rate.
6. *In situ* deformation revealed that the presence of Type-I boundary or Type-II boundary or martensitic islands have meager effect on joint efficiency. All the joints failed from buttering material and

fracture path was away from fusion boundary. Maximum bond strength with adequate ductility was obtained for WL 309. In this respect the use of Ni-base buttering material did not improve the bond strength significantly in comparison to 309L SS buttering material. For satisfactory weld strength without compromising ductility, it was desirable to have good solid solution strengthening of buttering material. Therefore, to obtain adequate joint efficiency for DMW consisting of LAS and 304LN SS, the preferred buttering material is 309L SS.

ACKNOWLEDGMENT

The authors are indebted to Director_CSIR-NML for providing infrastructural facilities to carry out the investigation and providing permission to publish the work.

REFERENCES

1. C. Jang, J. Lee, J.S. Kim, and T.E. Jin: *Int. J. Press. Vessel. Pip.*, 2008, vol. 85, pp. 635–46.
2. S. Missori and C. Koerber: *Weld. J.*, 1997, vol. 76, pp. 125s–34s.
3. J.N. DuPont, J.N. Lippold, and S.D. Kiser: *Welding Metallurgy and Weldability of Ni-Base Alloys (Chap. 7)*, Wiley, Hoboken, 2009, pp. 327–76.
4. A. Celik and A. Alasaran: *Mater. Charact.*, 1999, vol. 43, pp. 311–18.
5. H. Naffakh, M. Shamanian, and F. Ashrafizadeh: *J. Mater. Process. Technol.*, 2009, vol. 209, pp. 3628–39.
6. M. Sireesha, S.K. Albert, V. Shankar, and S. Sundaresan: *J. Nucl. Mater.*, 2000, vol. 279, pp. 65–76.
7. A. Wiltner, C. Linsmeier, and T. Jacob: *J. Chem. Phys.*, 2008, vol. 129, pp. 084704-1–10.
8. C. Pan and E. Zhang: *Mater. Charact.*, 1996, vol. 36, pp. 5–10.
9. H.S. Hosseini, M. Shamanian, and A. Kermanpur: *Mater. Char.*, 2011, vol. 62, pp. 425–31.
10. H. Naffakh, M. Shamanian, and F. Ashrafizadeh: *J. Mater. Proc. Technol.*, 2009, vol. 209, pp. 3628–39.
11. H.T. Lee, S.L. Jeng, C.H. Yen, and T.Y. Kuo: *J. Nucl. Mater.*, 2004, vol. 2004, pp. 59–69.
12. F. Matsuda and H. Nakagawa: *Trans. JWRI*, 1984, vol. 13, pp. 159–61.
13. T.W. Nelson, J.C. Lippold, and M.J. Mills: *Sci. Technol. Weld. Join.*, 1998, vol. 3, pp. 249–54.
14. K. Sharma, H.K. Khandelwal, V. Bhasin, and R. Chhibber: *Adv. Mater. Res.*, 2012, vol. 585, pp. 342–46.
15. https://inis.iaea.org/search/search.aspx?orig_q=RN:43001715.
16. C.D. Lundin: *Weld. J.*, 1982, vol. 61, pp. 585s–635s.
17. R.L. Klueh and J.F. King: *Weld. J.*, 1982, vol. 61, pp. 302–11.
18. W.J. Mills and C.M. Brown: *Metall. Mater. Trans. A*, 2001, vol. 32A, pp. 1161–74.
19. J. Gallego, A.R. Rodrigues, C.L.F. DeAssis, and L. Montanari: *Mater. Res.*, 2014, vol. 17, pp. 22–25. DOI:10.1590/S1516-14392013005000199.
20. L. Yang, X. Dang, M. Li, and N. Ji: *Proceedings of 2nd International Conference on Electronic and Mechanical Engineering and Information Technology (EMEIT 2012)*, Shenyang Liaoning, China, Prof. B. Wu, ed., Atlantis Press, Paris, pp. 697–700.
21. N. Wang, S. Mokadem, M. Rappaz, and W. Kurz: *Acta Mater.*, 2004, vol. 52, pp. 3173–82.
22. T.Y. Kuo and H.T. Lee: *Mater. Sci. Eng. A.*, 2002, vol. 338, pp. 202–12.
23. R. Dehmolaie, M. Shamanian, and A. Kermanpur: *Mater. Charact.*, 2008, vol. 59, pp. 1447–54.
24. W.F. Savage, E.F. Nipess, and E.S. Szekeres: *Weld. J.*, 1976, vol. 55, pp. 260–68.
25. C. Pan, R. Wang, and J. Gui: *J. Mater. Sci.*, 1990, vol. 25, pp. 3281–85.

26. T.W. Nelson, J.C. Lippold, and M.J. Mills: *Weld. J.*, 1999, vol. 78, pp. 329s–37s.
27. M.D. Rowe, T.W. Nelson, and J.C. Lippold: *Weld. J.*, 1999, vol. 78, pp. 31s–37s.
28. J.N. DuPont and C.S. Kusko: *Weld. J.*, 1996, vol. 86, pp. 51s–54s.
29. R.E. Reed-Hill: *Physical Metallurgy Principals (Chap. 18)*, 2nd ed., East West Press Pvt. Ltd., Delhi, 1973, pp. 701–748.
30. S.S.F. DeDafe, F.L. Sicupira, F.C.S. Matos, N.S. Cruz, D.R. Moreira, and D.B. Santos: *Mater. Res.*, 2013, vol. 16, pp. 1229–36.
31. T.W. Nelson, J.C. Lippold, and M.J. Mills: *Weld. J.*, 2000, vol. 79, pp. 267–77.
32. M.W.A. Rashid, M. Gakim, Z.M. Rosli, and M.A. Azam: *Int. J. Electrochem. Sci.*, 2012, vol. 7, pp. 9465–77.
33. <http://www.steel-grades.com/Steel-Grades/Mould-Steel/aws-enicrfe-3.html>.
34. G.D. Huang, D.K. Matlock, and G. Krauss: *Metall. Trans. A*, 1989, vol. 20A, pp. 1239–46.
35. R.E. Schramm and R.P. Reed: *Metall. Trans. A*, 1975, vol. 6A, pp. 1345–51.
36. D.J. Siegel: *Appl. Phys. Lett.*, 2005, vol. 87, pp. 121901-1–3.
37. A.M. Shariatpanahi: *Adv. Mater. Res.*, 2009, vol. 83-86, pp. 449–56.